

The boundary entropy function for interface conformal field theories

Evangelos Afxonidis^{a,b} and Andreas Karch^b

^a*Department of Physics and Instituto de Ciencias y Tecnologías Especiales de Asturias (ICTEA), Universidad de Oviedo, c/ Leopoldo Calvo Sotelo 18, ES-33007, Oviedo, Spain*

^b*Weinberg Institute, Department of Physics, University of Texas, 2615 Speedway, Austin, TX 78712, USA*

E-mail: afxonidisevangelos@uniovi.es, karcha@utexas.edu

ABSTRACT: In 1+1 dimensional conformal field theory with a boundary the boundary contribution to the entanglement entropy is determined by a single number g effectively counting the boundary degrees of freedom. In contrast, in 1+1 dimensional interface CFTs the corresponding quantity is a non-trivial *function* depending on the position of the interval relative to the interface, giving access to much more detailed information about the defect. In this work we determined this g -function in several examples using holography and derive some of its basic properties from holography and strong subadditivity.

Contents

1	Introduction	1
2	Examples of $g_{\text{eff}}(l_L/l_R)$	4
2.1	Setup	4
2.2	Super-Janus and non-universality of g_{eff}	6
2.3	Updates on Standard Janus	9
2.4	Asymptotic behavior of solutions	11
2.4.1	Janus	11
2.4.2	Super-Janus	12
2.5	The RS braneworld	13
2.6	ICFT holographic entanglement and interface entropy	14
3	Constraints on $g_{\text{eff}}(l_L/l_R)$	16
3.1	Entropic g_{eff} -theorem	17
3.2	Holographic SSA	19
A	Entropic quantities under KK compactification	19
A.1	Boundary entropy g	19
A.2	Effective central charge c_{eff}	20

1 Introduction

The foundational work of Cardy catalyzed the study of Boundary Conformal Field Theories (BCFTs) [1], establishing profound connections with both condensed matter physics and string theory. More recently, Interface Conformal Field Theories (ICFTs) have garnered attention as well [2], albeit to a lesser extent. An ICFT describes a system in which a conformally invariant interface joins two, potentially distinct, Conformal Field Theories (CFTs) with differing central charges.

ICFTs can be viewed as a specialized subclass of BCFTs, preserving analogous symmetries. Utilizing the folding trick, acting with $x \rightarrow -x$ on half of space, one can transform the ICFT setup into a BCFT framework. While this is formally an identity, certain physical quantities that appear natural before folding lead to questions that look strange in the folded picture and so have escaped attention when focusing on BCFTs.

One simple to understand example of such a quantity is the energy transmission coefficient [3, 4] T , which clearly is only defined for the case of interfaces, not for boundaries. In this work we will focus on another such ICFT specific quantity, the entanglement entropy (EE) associated with an interval \mathcal{A} crossing the interface. The interval is taken to have

total length l , with the portions of the interval on either side of the interface having length l_L and l_R respectively.

Such an interface crossing interval \mathcal{A} can be folded into an interval terminating on the BCFT boundary provided l_L and l_R are equal. Within this context, the entanglement entropy (EE) can be computed using the replica method [5], yielding

$$S_{\mathcal{A}} = \frac{c_L + c_R}{6} \log \frac{l}{\epsilon} + \log g, \quad (1.1)$$

where $l = l_L + l_R$ denotes the total interval length, c_L and c_R are the central charges on either side of the interface, so that $c_L + c_R$ is the central charge of the BCFT after folding, and ϵ represents the UV cutoff.

The number $\log g$ appearing in (1.1) is a pivotal quantity characterizing defects or boundaries and is referred to as the boundary entropy [5], which had previously been introduced using a thermodynamic definition in [6]. $\log g$ measures the degrees of freedom localized at a defect and serves as a boundary analogue of the central charge c . While g is known in many free or solvable examples, calculating the boundary entropy in strongly coupled system becomes challenging. However, holography provides a powerful tool for this purpose by enabling the computation of the boundary entropy via the holographic EE (HEE) prescription [7].

In the case of a generic asymmetric ICFT interval, g in (1.1) gets replaced with an effective g_{eff} -function [8, 9], which depends non-trivially on the ratio l_L/l_R . Only for $l_L = l_R$ does g_{eff} reduce to the standard g , $g_{\text{eff}}(1) = g$. The degenerate case with either l_L or l_R vanishing is even more intriguing, in that case even the coefficient of the log divergent term changes, and one of the central charges in (1.1) gets replaced by an effective central charge c_{eff} [9–11]. This effective central charge has played a crucial role in much recent work on this subject [12–14], where it was shown that it can be thought of as a transmission coefficient for quantum information that obeys interesting bounds, especially when compared to the transmission coefficient for energy. In contrast, in this work we will stay away from this extreme limit and instead focus on g_{eff} , which governs the behavior of the EE at finite l_L and l_R .

In this work we'll focus entirely on the somewhat special case where the central charge c on the two sides of the interface is the same, $c_L = c_R = c$. Very little is known about g_{eff} even in this limited context. It has previously been analyzed in few explicit holographic examples such as the Janus and RS braneworld solutions [15–17]. These studies revealed that g_{eff} indeed depends intricately on the ratio l_L/l_R of the intervals around the interface. The 3d Janus solution [18], a straightforward generalization of the original 5d Janus solution constructed in [19], is a fully backreacted type IIB supergravity solution asymptotically approaching $AdS_3 \times S^3 \times T^4$.¹ It is holographically dual to an interface theory where the conformal field theory on either side of the interface is a non-linear sigma model with a T^4/S_N target space. The marginal coupling corresponding to the T^4 size modulus remains constant in the two 1 + 1-dimensional half-spaces but exhibits a discontinuity across a planar 0 + 1-dimensional ace. The subcritical Randall-Sundrum (RS) braneworld model

¹The compactification manifold M_4 may alternatively be T^4 or K_3 , but T^4 offers a simpler dual SCFT.

[9, 20], by contrast, is based on Einstein gravity with a negative cosmological constant and includes a brane as matter content. For brane tensions below a critical value, the brane intersects the boundary along a timelike defect, with the regions on either side of the defect being empty AdS spaces. This setup provides a holographic dual to ICFTs, albeit as a bottom-up construction without explicit derivation from string theory.

In this holographic setting, a distinctive feature of g_{eff} is its sensitivity to the full geometry of the solution as encoded in the warp factor $e^{A(r)}$, as extensively analyzed in the context of the super-Janus solution in this paper. Super-Janus solutions are once again type IIB supergravity configurations asymptotic to $AdS_3 \times S^3 \times T^4$, and, like 3d Janus itself, are dual to marginal deformations of two-dimensional $\mathcal{N} = (4, 4)$ SCFTs. Unlike the simpler Janus solution, the super-Janus metric involves a fibration over a Riemann surface, complicating its dimensional reduction to three dimensions [21]. From the point of view of the CFT, extra terms are added on the interface to ensure that the interface preserves half of the supersymmetries. In contrast, in the standard 3d Janus solution, the interface, while preserving conformal invariance, breaks all supersymmetries.

To conduct our analysis, we employ HEE tools [7, 22, 23]. The AdS/CFT correspondence, first proposed in [24], posits an equivalence between gravity in a $d + 1$ -dimensional AdS spacetime and a d -dimensional CFT [24, 25]. Within this framework, the EE $S_{\mathcal{A}}$ of an entangled region \mathcal{A} is geometrically computed via the area of an extremal surface $\Gamma_{\mathcal{A}}$, denoted as $|\Gamma_{\mathcal{A}}|$, homologous to \mathcal{A} and terminating on its boundary in AdS:

$$S_{\mathcal{A}} = \frac{|\Gamma_{\mathcal{A}}|}{4G}, \quad (1.2)$$

where G is the Newton constant.

A cornerstone of quantum information theory is the strong subadditivity inequality (SSA) [26], expressed as

$$\Delta S = S_A + S_B - S_{A \cap B} - S_{A \cup B} \geq 0. \quad (1.3)$$

HEE offers a geometrical derivation of SSA, rooted in the triangle inequality of Euclidean geometry [27]. Furthermore, SSA underpins the derivation of g -theorems in BCFTs [28]. In this paper, leveraging SSA arguments, we propose a g_{eff} -theorem for the interface entropy. Additionally, we provide holographic computations for cases involving interfaces whose bulk theories exhibit conformal invariance.

This paper is organized as follows. Section 2 explores g_{eff} in three examples—the super-Janus, Janus, and RS braneworld solutions—emphasizing its dependence on the spacetime warp factor. We also derive a compact form of the interface entropy in terms of l_L and l_R . Section 3 introduces the g_{eff} , offering a holographic perspective. We present technical details, in particular the dimensional reduction of the boundary entropy g and the effective central charge c_{eff} under KK compactification, in appendix A.

2 Examples of $g_{\text{eff}}(l_L/l_R)$

2.1 Setup

Holographic ICFTs are often described by three-dimensional gravity duals. Consistency within string theory suggests that these duals typically correspond to ten-dimensional spacetimes with seven compactified dimensions. In some cases, the internal space is non-trivially fibered over the relevant three-dimensional spacetime, as seen in the gravitational duals of 3 + 1 dimensional supersymmetric Janus solutions introduced in [29]. The starting point for the construction of conformal defect spacetimes in 2 + 1 dimensions is given by a metric of the form

$$ds^2 = e^{A(r)} \frac{dx^2 - dt^2}{x^2} + dr^2. \quad (2.1)$$

This configuration can be interpreted as AdS_2 slices within an AdS_3 spacetime. The two-dimensional slices depend on the holographic direction through the warp factor $A(r)$. The case of pure AdS_3 corresponds to the presence of a completely transparent defect on the 1 + 1 dimensional boundary and its warp factor is given by

$$e^{A(r)} = \cosh(r). \quad (2.2)$$

The boundary of AdS_3 consists of two copies of AdS_2 which are approached as $r \rightarrow \pm\infty$, with an interface bridging the two regions. A convenient description that will occasionally be employed is provided by the Poincaré coordinates, in which the boundary is located at $z = 0$

$$ds^2 = \frac{1}{z^2} (-dt^2 + dy^2 + dz^2). \quad (2.3)$$

The two coordinate systems (2.1) and (2.3) are related by the following transformations

$$z = \frac{x}{\cosh r}, \quad y = x \tanh r. \quad (2.4)$$

In this paper, we focus on the case where the intervals on the left and right of the interface are unequal. This disparity can be encoded in the integration constant c_s arising from the scale isometry, $x \rightarrow \lambda x$, of the AdS_2 slices.

Consider $l_L \equiv \lim_{r \rightarrow -\infty} x(r)$ the interval lying to the left of the interface, and $l_R \equiv \lim_{r \rightarrow \infty} x(r)$ the interval on the right. To compute the minimal RT surface, as prescribed in [7], we define the Lagrangian as follows

$$\mathcal{L} = \sqrt{\frac{e^{2A}}{x^2} (x')^2 + 1}. \quad (2.5)$$

The associated Noether charge is

$$c_s = \frac{\partial \mathcal{L}}{\partial x'} \frac{\partial(\lambda x)}{\partial \lambda} = \frac{e^{2A} x'}{\sqrt{x^2 + e^{2A} (x')^2}}. \quad (2.6)$$

which solving for x' yields

$$\frac{x'}{x} = \pm \frac{c_s e^{-A}}{\sqrt{e^{2A} - c_s^2}}. \quad (2.7)$$

We can immediately obtain the constraint

$$0 \leq |c_s| \leq e^{A^*}, \quad (2.8)$$

where e^{A^*} is the minimal warp factor. Since (2.7) has a sign ambiguity nothing is lost by restricting to positive c_s . For the case of pure AdS_3 case we have $e^{A^*} = 1$. Without loss of generality we can choose the positive sign in (2.7). The on-shell Lagrangian for the positive solution of (2.7) is given by

$$\mathcal{L} = \frac{1}{\sqrt{1 - c_s^2 e^{-2A}}}. \quad (2.9)$$

Depending on what value c_s takes, we can distinguish different cases for the extremal RT surface:

- For $c_s = 0$, we get from (2.7) that $x' = 0$ and hence $x = l_R = \text{const}$, due to the asymptotics at $r \rightarrow \infty$. That is the case where $l_R = l_L = l/2$, i.e. the interval around the interface is symmetric. This case corresponds to the standard BCFT result, where the standard folding trick yields $S = \frac{2c}{6} \log(l/\epsilon)$ for the entanglement entropy.
- For $0 < c_s < e^{A^*}$, we have that $1/\sqrt{1 - c_s^2 e^{-2A}}$ is always positive and thus we fall into the case of $l_R \geq l_L$ if we chose the plus sign in (2.7), since x' is strictly positive in this case, and $l_L \geq l_R$ if we chose the minus sign. Either way this realizes the case of a non-trivial ICFT setup. Notice that the folding trick cannot be usefully applied here. The non-symmetric interval would fold to a configuration with 3 regions, where all degrees of freedom are traced out in one, some in a second, and none in the third. This is not a standard EE setup. Without loss of generality we limit ourselves to the case that $l_R \geq l_L$.
- When c_s takes the maximum value $c_s = e^{A^*}$ the solution truncates at $r = 0$ and we get not just two but actually *four* different solutions depending on the choice of sign in (2.7) and whether we look at positive or negative r . Focusing on positive r and choosing the plus sign in (2.7) yields the case of $l_L = 0$. This is because, (2.7) diverges at $r \rightarrow 0$ unless $x = 0$ at that point. The plus sign in (2.7) allows for a solution which terminates at $x(0) = 0$ with x smoothly increasing to $x(\infty) = l_R$. This solution corresponds to an RT surface ending on the interface with $l_L = 0$. The solution with the minus sign will play a prominent role when we revisit the case of the bosonic Janus.
- For $c_s > e^{A^*}$ one finds RT surfaces which have two endpoints on the same side of the interface and so are of no interest for our study.

Therefore, we see that the value of c_s affects the length of the intervals around the interface and thus the EE computation.

2.2 Super-Janus and non-universality of g_{eff}

In this section we study the holographic dual of the 2D supersymmetric Janus ICFT, originally constructed in [30]. It arises as a solution of type IIB supergravity, which is locally asymptotic to $AdS_3 \times S^3 \times M_4$. The compactification manifold M_4 can be either T^4 or K_3 , corresponding to the target space of the dual CFT. For simplicity we consider the case of T^4 .

The ten-dimensional metric is a fibration of $AdS_2 \times S^2 \times T^4$ over a Riemann surface Σ and given by

$$ds_{(10)}^2 = f_1^2 ds_{AdS_2}^2 + f_2^2 ds_{S^2}^2 + f_3^2 ds_{T^4}^2 + \rho^2 ds_{\Sigma}^2 \quad (2.10)$$

which contains five parameters θ, ψ, L, k and b . ψ parametrizes the jump of the six-dimensional dilaton through the interface, while θ the jump of the axion. The various functions in the metric above are given by two meromorphic function and two harmonic functions [31]. Note that setting $\theta = 0$ and $\psi = 0$ gives the $AdS_3 \times S^3$ vacuum.

The goal is to reduce the ten-dimensional system down to a three-dimensional geometry. One can achieve this by first compactifying (2.10) over T^4 down to six dimensions. The resulting metric is of the form $AdS_2 \times S^2 \times \Sigma$ and be further reduced to three dimensions by first compactifying on S^2 and then on the compact part of Σ . Notice that all functions depend on the complex coordinate on the fibration Σ and one needs to be attentive when KK reducing [21]. The resulting three-dimensional metric is given by

$$ds_{(3)}^2 = R^2 \left(\frac{\cosh^2(r + \psi)}{\cosh^2 \psi \cosh^2 \theta} ds_{AdS_2}^2 + dr^2 \right) = R^2 \left(e^{2A(r)} ds_{AdS_2}^2 + dr^2 \right). \quad (2.11)$$

with the AdS_3 radius and the warp factor given by

$$R^2 = 2L \cosh \psi \cosh \theta, \quad e^{A(x)} = \frac{\cosh(r + \psi)}{\cosh \psi \cosh \theta} \quad (2.12)$$

Following [15] we can find that the integration constant c_s takes the following values

$$0 \leq c_s \leq e^{A_*} = \frac{1}{\cosh \psi \cosh \theta}. \quad (2.13)$$

Furthermore, for the case of asymmetric intervals around the interface, $0 < c_s < e^{A_*}$, substituting the super Janus warp factor (2.12) into the equations of motion (2.7) yields

$$\frac{x(r)}{x_0} = \exp \left[\pm \tanh^{-1} \left(\frac{c_s \sinh(r + \psi)}{\sqrt{-c_s^2 + \frac{\cosh^2(r + \psi)}{\cosh^2 \psi \cosh^2 \theta}}} \right) \cosh \theta \cosh \psi \right]. \quad (2.14)$$

By considering the $x \rightarrow \pm\infty$ limits of (2.14), one can determine

$$l_R = r_0 \exp \left[\tanh^{-1} (c_s \cosh \theta \cosh \psi) \cosh \theta \cosh \psi \right], \quad (2.15)$$

$$l_L = r_0 \exp \left[-\tanh^{-1} (c_s \cosh \theta \cosh \psi) \cosh \theta \cosh \psi \right]. \quad (2.16)$$

To compute the regulated area \mathcal{A} , we must integrate the on-shell Lagrangian, incorporating the super-Janus warp factor. Analogous to [15], the asymptotic value of the super Janus warp factor (2.12) takes the form

$$e^A \sim \frac{1}{2 \cosh \theta \cosh \psi} e^r = \frac{x}{z}. \quad (2.17)$$

Therefore, the regulated limits are given by

$$r_c^\pm = \log \left(\frac{2l_{R/L}}{\epsilon} \right) + \log (\cosh \psi \cosh \theta). \quad (2.18)$$

The regulated limits are consistent, as the g -number for the super Janus configuration can be computed as

$$\mathcal{A}_{c_s=0} = \int_{-x_c^-}^{x_c^+} R(\mathcal{L} = 1) = 2R \log \left(\frac{l}{\epsilon} \right) + 2R \log \cosh \psi \cosh \theta. \quad (2.19)$$

This aligns with the 3D calculation of the g -number performed in appendix A and the 6D analysis presented in [31].

For $0 < c_s < \frac{1}{\cosh \psi \cosh \theta}$, the regulated area \mathcal{A} is determined through numerical integration of the on-shell Lagrangian (2.9) with the super-Janus warp factor. For arbitrary values of ψ and $\theta = 0$ in the super-Janus solution with $L = 1$, the result is given in figure 1.

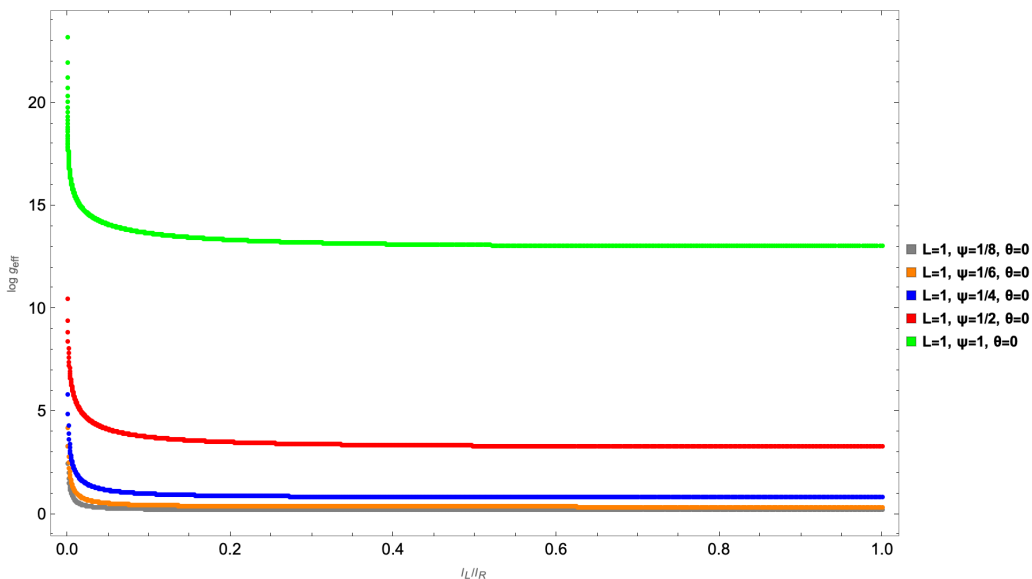


Figure 1. Effective interface entropy for the super-Janus solution as a function of the ratio l_L/l_R .

The interface entropy $\log g_{\text{eff}}$ is computed as the difference between the minimal RT surface in the super-Janus case and the empty AdS, $\mathcal{A}(\theta = 0, \psi \neq 0) - \mathcal{A}(0, 0)$, similar to [8]. Crucially, all curves diverge when the ratio approaches zero, indicating that the interval becomes maximally asymmetric. This is in contrast to the Janus solution as in

[15], where the curves blow up for different values of the ratio. We will analyze the cause of this difference in the next section. On the other hand, the curves attain their boundary entropy values as the ratio approaches one.

An intriguing check would be to determine whether the interface entropy is universal, in that one may contemplate that the function $g_{\text{eff}}(l_L/l_R)$ is fixed by conformal invariance in terms of the symmetric value at $l_L = l_R$. To investigate this, we can compare the interface entropies of the Janus [15] and super-Janus solutions as in figure 1, and assess whether the corresponding curves coincide for the same boundary entropy. Recall that the boundary entropy of the Janus solution is given by [8]

$$\log g = \frac{1}{\sqrt{1 - 2\gamma^2}}. \quad (2.20)$$

Therefore, the relation between the two boundary entropies is given by

$$\cosh^2 \psi = \frac{1}{\sqrt{1 - 2\gamma^2}}, \quad (2.21)$$

where we have set $\theta = 0$ and $R = 1$. We would like to compare the interface entropy $\log g_{\text{eff}}$ for the two solutions as a function of the field theory quantity l_L/l_R on the boundary. It is noteworthy that while $\log g_{\text{eff}}$ can be plotted analytically in terms of the integration constant c_s , mapping c_s to the ratio l_L/l_R is highly non-trivial for both the Janus and super-Janus solution. Consequently, we employ numerical methods to perform this mapping, as illustrated in figure 2.

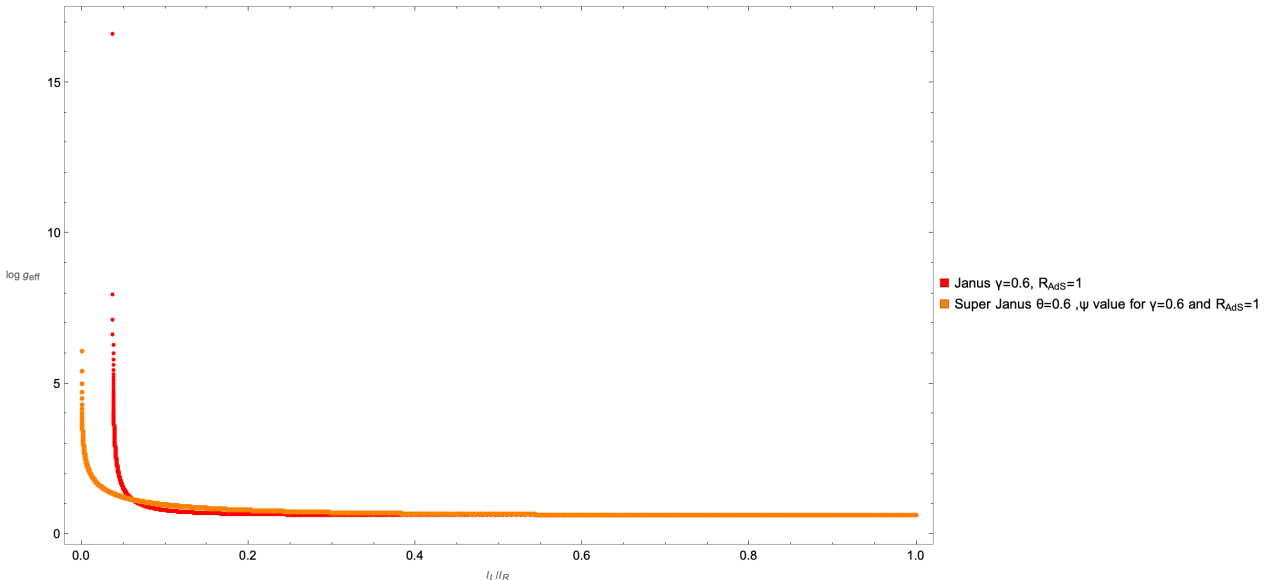


Figure 2. Effective interface entropy as a function of the ratio l_L/l_R for both the Janus and super-Janus solution. Note that both curves have the same boundary entropy g but they diverge for different values of the ratio.

It is evident that the curves diverge as the interval approaches maximal asymmetry. Throughout this analysis, we have assumed $l_R \geq l_L$, such that the ratio spans the range from 0 to 1. Notably, both curves converge to the same boundary entropy g on the right-hand side, in agreement with established results [31]. This consistency renders them a suitable basis for examining the non-universality of the effective entropy at the interface $\log g_{\text{eff}}$ for the Janus and super-Janus solutions. We thus conclude that the interface entropy is non-universal, as it is explicitly sensitive to the full warp factor $e^{A(r)}$. In other words, while the value of g at $l_L = l_R$ is fixed, the functional dependence of $g_{\text{eff}}(l_L/l_R)$ is not governed by conformal invariance but rather by the details of the underlying theory.

2.3 Updates on Standard Janus

In this section, we provide updates on the interface entropy of the Janus solution previously discussed in [15]. The Janus solution was originally introduced as a 3+1 dimensional ICFD with its asymptotically $AdS_5 \times S^5$ supergravity dual in [19], with the 1+1 dimensional version dual to an interface in asymptotically $AdS_3 \times S^3 \times T^4$ presented in [32]. This non-supersymmetric Janus solution is notably simpler than its supersymmetric counterpart, as the three-dimensional metric appears as a direct product factor in the ten-dimensional metric. The compactified three-dimensional part is described by the Einstein-Hilbert action plus a scalar field ϕ and given by

$$ds_{(3)}^2 = dr^2 + \frac{1}{2} \left(1 + \sqrt{1 - 2\gamma^2} \cosh(2r) \right) ds_{AdS_2}^2, \quad (2.22)$$

where $|\gamma| \leq 1/\sqrt{2}$. The dilaton is given by [31]

$$\phi(r) = \phi_0 + \frac{1}{\sqrt{2}} \log \left(\frac{1 + \sqrt{1 - 2\gamma^2} + \sqrt{2}\gamma \tanh r}{1 + \sqrt{1 - 2\gamma^2} - \sqrt{2}\gamma \tanh r} \right). \quad (2.23)$$

When $\gamma = 0$, the dilaton becomes constant ϕ_0 and the metric reduces to pure AdS_3 . When $\gamma = 1/\sqrt{2}$, the spacetime is simply given by $\mathbb{R} \times AdS_2$. Let us define $\xi \equiv \sqrt{1 - 2\gamma^2}$. Then, the Janus warp factor is

$$e^{A(r)} = \sqrt{(1 + \xi \cosh 2r)/2}. \quad (2.24)$$

The integration constant c_s is then bounded by

$$0 \leq c_s \leq \sqrt{\frac{1 + \xi}{2}}. \quad (2.25)$$

As discussed in section 2.2, a significant distinction arises between the interface entropy profiles of the Janus and super-Janus cases. Specifically, the curves corresponding to different values of γ as analyzed in [15], exhibit divergence at distinct values of the ratio l_L/l_R . This behavior can be interpreted from a disconnected solution. Plotting the ratio l_L/l_R against the integration constant c_s one obtains figure 3.

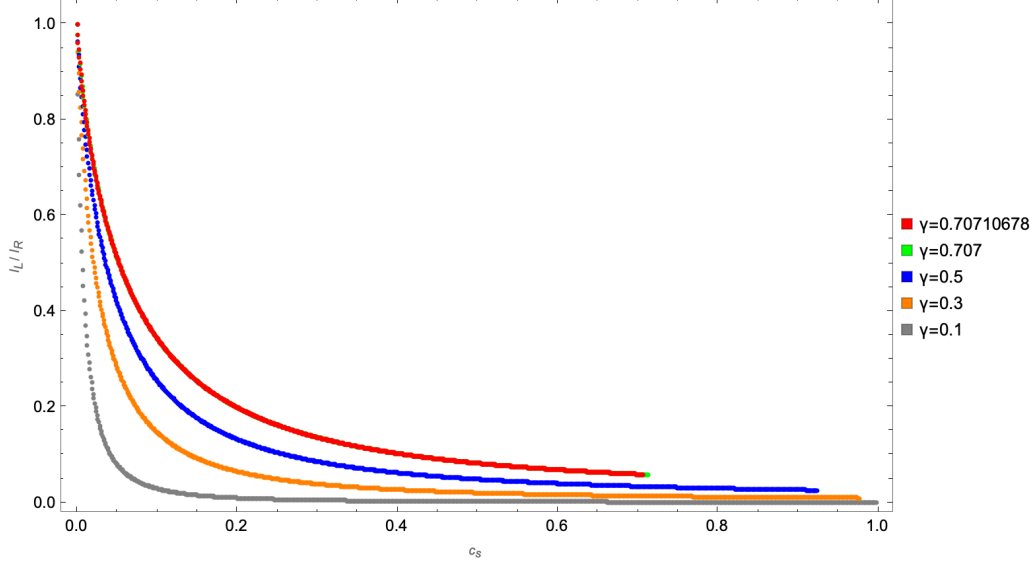


Figure 3. Plot of l_L/l_R with respect to the integration constant c_s . Notice that the curves acquire a gap in that they terminate at some value of c_s for every given γ .

The curves develop a gap, for example the curve for $\gamma = 0.70710678$ terminates at a finite value of the ratio rather than approaching zero. This behavior occurs precisely at the same value of the ratio, where the curves in [15] exhibit a divergence. This observation suggests the emergence of disconnected RT surfaces that dominate for smaller values of l_L/l_R and larger values of c_s .

The relevant disconnected solution is also given by $c_s = e^{A^*}$, just like the $l_L = 0$ case, but this time with the minus sign in (2.7). In this case $x(0)$ can not vanish like it did in the case of an RT surface ending on the interface, since for this sign choice it has to be *larger* than $x(\infty)$. The divergence in (2.7) instead will force x to diverge as $r \rightarrow 0$. To verify this, one can substitute this specific value of c_s into the differential equation (2.7). The solution describes an RT surface that starts at the boundary at $r \rightarrow \infty$, $x = l_R$ and then reaches straight down into the bulk towards the Poincare patch horizon. To describe the full RT surface we need a second such horizon crossing surface attached to $x = l_L$ at $r = -\infty$: the full RT surface is disconnected.

We can explicitly write down these disconnected solutions. Solving for x yields

$$x(r) = x_0 \sqrt{\frac{1+\chi}{\chi-1}} e^{\frac{1}{\sqrt{\xi}}}, \quad \chi \equiv \frac{\sqrt{\xi+1} \cosh(r)}{\sqrt{\xi} \cosh(2r) + 1}. \quad (2.26)$$

which indeed has the properties that

$$\begin{aligned} \lim_{r \rightarrow 0^+} x(r) &\rightarrow \infty, \\ \lim_{r \rightarrow \infty} x(r) &= e^{\frac{i\pi}{2\sqrt{\xi}}} \left(\frac{\sqrt{2}\sqrt{\frac{1}{\xi} + 1} - 2}{\sqrt{2}\sqrt{\frac{1}{\xi} + 1} + 2} \right)^{\frac{1}{2\sqrt{\xi}}} = l_R. \end{aligned} \quad (2.27)$$

This disconnected solution starts to kick in after l_L/l_R reaches the gap as seen in figure 3, and subsequently dominates the connected solution given by $c_s = -e^A$.

This disconnected solution leads to a logarithmic IR divergence near the Poincare Patch horizon. To understand this behavior, we examine the on-shell Janus Lagrangian near $r = 0$ where $x \rightarrow \infty$. From (2.9) we see that the integrand of the area functional indeed diverges near $r = 0$ when $c_s e^{-2A_*} = 1$. To find the behavior near the singularity we can expand the warp factor near $r = 0$:

$$A(r) = A_* + \frac{1}{2}A''(0)r^2 + \mathcal{O}(r^3) \quad (2.28)$$

and so the integrand of the on-shell action goes as

$$\mathcal{L} \sim \sqrt{\frac{2}{A''(0)}} \frac{1}{r}. \quad (2.29)$$

Clearly this gives a logarithmically divergent contribution to the area of the disconnected RT surface. One should note that this is really a large x and hence IR divergence. The total length of the geodesic reaching towards the Poincare patch horizon picks up an infinite length from the region near the horizon in addition to the standard UV divergence from near the boundary. As such, the disconnected solution always has a larger area than the connected solution when the latter exists, as the connected solution is IR finite. In the Standard Janus solution these disconnected solutions have to fill the gap in which the connected solution does not exist. In this regime the EE is very large and sensitive to the IR cutoff.

2.4 Asymptotic behavior of solutions

In this section, we investigate the behavior of the Janus and super-Janus solutions as the ratio l_L/l_R approaches its critical blow up value or zero.

2.4.1 Janus

We can expand the solution near $c_s = 0$ to compute the next-to-leading order correction in boundary entropy g . To do this, we substitute the Janus warp factor into the on-shell Lagrangian and expand for small c_s . By integrating and applying the regularized limits, one obtains

$$\begin{aligned} \mathcal{A} &= \left[r + \frac{c_s^2 \tan^{-1} \left(\frac{(\xi-1) \tanh(r)}{\sqrt{\xi^2-1}} \right)}{\sqrt{\xi^2-1}} + \mathcal{O}(c_s^3) \right] \Big|_{-r_c^-}^{r_c^+} \\ &= 2 \log(l/\epsilon) - \log \xi + \frac{c_s^2}{\sqrt{1-\xi^2}} \log \left[\frac{(\xi-1) \left(\frac{2l^2}{l^2+\epsilon^2\xi} - 1 \right) - \sqrt{1-\xi^2}}{-(\xi-1) \left(\frac{2l^2}{l^2+\epsilon^2\xi} - 1 \right) - \sqrt{1-\xi^2}} \right] + \mathcal{O}(c_s^3). \end{aligned} \quad (2.30)$$

The first two terms are in agreement with [15], while the latter serves as a correction for small c_s . It can be easily checked that the latter term is positive and real, namely, the interface entropy is still positive and real.

2.4.2 Super-Janus

Let us now turn to the super-Janus solution. In this case, we have found that for $0 < c_s < e^{A^*}$, there are connected solutions that yield minimal RT surfaces. Furthermore, one can easily verify that no disconnected solutions exist when $c_s = \pm e^{A^*}$, in contrast to the Janus solution as discussed in section 2.3. It is worth noting that the regulated limits r_c^\pm given by (2.18), have the same structure as those used in pure AdS setups, with the only difference being the additional ψ and θ dependent terms. This suggests that the super-Janus solution is a shifted version of pure AdS. Consequently, this immediately implies that the variation of the minimal area with respect to l_L and l_R follows a similar pattern

$$\delta\mathcal{A} = \mathcal{L}|_{r=x_c^+} \frac{\delta x_c^+}{\delta l_R} \delta l_R - \mathcal{L}|_{r=-x_c^-} \frac{\delta(-x_c^-)}{\delta l_L} \delta l_L, \quad (2.31)$$

which yields

$$\frac{\delta x_c^\pm}{\delta l_{R/L}} = \frac{1}{l_{R/L}}, \quad (2.32)$$

resulting in

$$\mathcal{A} = \log\left(\frac{l_L}{\epsilon}\right) + \log\left(\frac{l_R}{\epsilon}\right) + \text{const} = 2 \log\left(\frac{l}{\epsilon}\right) + \text{const}. \quad (2.33)$$

This minimal area gives rise to the universal $\frac{\epsilon}{3} \log l$ term of the EE.

We also aim to examine the asymptotic behavior of the super-Janus solution near $c_s = 0$ and at the critical value where the curves exhibit a divergence. Starting with the former, we can expand the solution around $c_s = 0$ to compute the next-to-leading order correction to the boundary entropy for the super-Janus solution. To do so, we substitute the super-Janus warp factor into the Lagrangian and perform an expansion for small c_s . After integrating and applying the regularized limits, the minimal area is found to be

$$\begin{aligned} \mathcal{A} &= \left(r + \frac{1}{2} c_s^2 \cosh^2 \theta \cosh^2 \psi \tanh(r + \psi) + \mathcal{O}(c_s^3) \right) \Big|_{-r_c^-}^{r_c^+} \\ &= 2 \log\left(\frac{l}{\epsilon}\right) + 2 \log(\cosh \theta \cosh \psi) + (c_s \cosh \theta \cosh \psi)^2 \left(\frac{l^2}{\epsilon^2 e^{2\psi} + l^2} - \frac{\epsilon^2}{\epsilon^2 + l^2 e^{2\psi}} \right) + \mathcal{O}(c_s^3) \end{aligned} \quad (2.34)$$

Similar to the Janus case, the first two terms are in agreement with [31], while the latter serves as a correction for small c_s . It can, once again, be easily verified that the latter term is both positive and real, ensuring that the interface entropy remains positive and real.

Finally, we perform an expansion near the blow-up point. In this vicinity, we express c_s as $e^{A^*} - \delta$, where δ is small. Expanding the minimal area for small δ , we find a divergence of the form

$$\mathcal{A} \sim f(\log \delta), \quad (2.35)$$

which indicates the divergence as $\delta \rightarrow 0$, signaling the blow-up behavior, as seen in figure 1.

2.5 The RS braneworld

One example extensively studied in [15] is the subcritical Randall-Sundrum (RS) braneworld [9, 20]. This model, based on Einstein gravity with a negative cosmological constant and matter in the form of a brane, is a simple solution in general relativity. The brane is a thin relativistic sheet with a constant energy density, characterized by its tension. For tensions below a critical value, the brane intersects the boundary along a time-like defect, with both sides of the defect being empty AdS. This setup allows the brane to be interpreted as a holographic dual of an ICFT, though as a bottom-up construction, the dual CFT cannot be explicitly derived from string theory.

For our purposes, we can view the RS braneworld as a particular instance of the warp factor

$$e^{A(r)} = \cosh(r - r_*). \quad (2.36)$$

The solution is defined piecewise for positive and negative values of r , where $r = 0$ is the location of the brane and r_* is the turnaround point, which is uniquely determined by the brane's tension T [33] as

$$\log g = \frac{2r_*}{4G} = \frac{c}{3} \tanh^{-1} \left(\frac{T}{2} \right). \quad (2.37)$$

The interface entropy was computed in [15] and given by

$$\log g_{\text{eff}}(c_s) = \frac{c}{3} \tanh^{-1} \frac{\sinh r_*}{\sqrt{\cosh^2 r_* - c_s^2}}. \quad (2.38)$$

Note that the connection between c_s and the ratio l_L/l_R is highly non-trivial. Therefore, one can numerically integrate the on-shell action for the RS warp factor (2.36). The subleading interface entropy is plotted in figure 4 with respect to the ratio l_L/l_R .

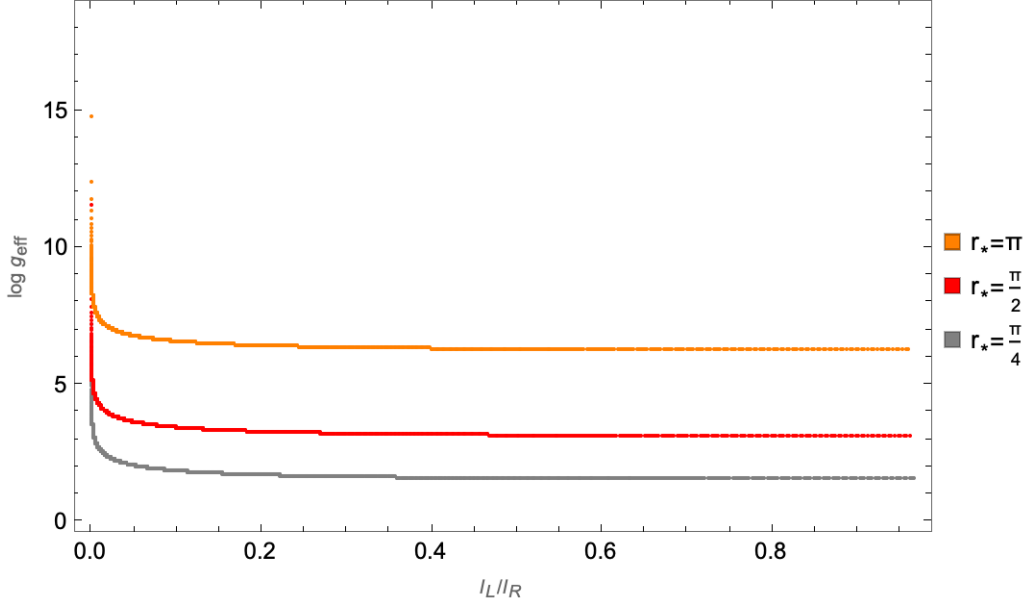


Figure 4. Effective interface entropy with respect to the ratio l_L/l_R , for different values of the turnaround point r_* . Once again, $\log g_{\text{eff}}$ is monotonically decreasing as a function of the ratio.

The curves all blow up when the ratio becomes zero, meaning that the interval become maximally asymmetric and they acquire the g -number values when $l_L = l_R$. It is important to note that all the previously discussed examples—the Janus, super-Janus, and RS braneworld solutions—result in a monotonically decreasing interface entropy. We provide further discussion on this in section 3.

2.6 ICFT holographic entanglement and interface entropy

For a two-dimensional ICFT, it is a well-established result that the entanglement entropy for non-zero intervals l_L and l_R on either side of the interface is given by

$$S = \frac{c}{3} \log(l/\epsilon) + \log g_{\text{eff}}(l_L/l_R), \quad (2.39)$$

where c denotes the central charge of the ICFT, l_L and l_R represent the lengths of the intervals to the left and right of the interface, ϵ is the UV cutoff and g_{eff} is the interface entropy.

For a general conformal defect metric of the form (2.1), the on-shell Lagrangian yields a minimal area of the form

$$\mathcal{A} = \int \frac{e^A}{\sqrt{e^{2A} - c_s^2}} dr. \quad (2.40)$$

Due to the divergence of the pure AdS warp factor $e^A = \cosh r$ on the asymptotically AdS boundaries $r = \pm\infty$ we have to regulate the integration limits as in [15]

$$r_c^+ = \log\left(\frac{2l_R}{\epsilon}\right), \quad r_c^- = \log\left(\frac{2l_L}{\epsilon}\right). \quad (2.41)$$

Then, the on-shell area (2.40) is given by

$$\begin{aligned}
\mathcal{A} &= \int_{-r_c^-}^{r_c^+} dr \frac{e^A}{\sqrt{e^{2A} - c_s^2}} \\
&= \int_{-r_c^-}^{\eta} dr \frac{e^A}{\sqrt{e^{2A} - c_s^2}} + \int_{\eta}^{r_c^+} dr \frac{e^A}{\sqrt{e^{2A} - c_s^2}} \\
&\approx \int_{-r_c^-}^{\eta} dr \frac{e^{-r}/2}{\sqrt{e^{-2r}/4 - c_s^2}} + \int_{\eta}^{r_c^+} dr \frac{e^r/2}{\sqrt{e^{2r}/4 - c_s^2}}.
\end{aligned} \tag{2.42}$$

By expanding the on-shell area for large negative and positive values of r , it is straightforward to identify that the divergent terms exhibit a logarithmic dependence, and are given by

$$\mathcal{A}_{\text{div}} = \log\left(\frac{2l_L}{\epsilon}\right) + \log\left(\frac{2l_R}{\epsilon}\right). \tag{2.43}$$

We have expanded the previous expression for small ϵ , allowing us to identify the interface entropy as

$$\log g_{\text{eff}}(c_s) = \lim_{\epsilon \rightarrow 0} \left[\frac{1}{4G_N} \int_{-r_c^-}^{r_c^+} \frac{e^A}{\sqrt{e^{2A} - c_s^2}} dr - \log\left(\frac{2l_L}{\epsilon}\right) - \log\left(\frac{2l_R}{\epsilon}\right) \right]. \tag{2.44}$$

Notice that the mapping of c_s to the ratio l_L/l_R is highly non-trivial contingent on the specific details of the theory. In the symmetric case ($c_s = 0$), equation (2.44) simplifies to the boundary entropy expression derived in [34].

Moreover, we can find a general form relating the integration constant c_s and the ratio l_L/l_R . To establish this, we begin by considering the differential equation given in (2.7), which can be reformulated as

$$\frac{d \log x(r)}{dr} = \frac{c_s e^{-A}}{\sqrt{e^{2A} - c_s^2}}. \tag{2.45}$$

Integrating both sides yields

$$\frac{l_L}{l_R} = \exp\left(-\int_{-\infty}^{\infty} \frac{c_s e^{-A}}{\sqrt{e^{2A} - c_s^2}} dr\right). \tag{2.46}$$

This result not only shows the dependence of c_s on the geometry but also provides an intuition on how the ratio l_L/l_R changes with respect to c_s .

One notable case where we can write down an analytical relation between the integration constant c_s and the ratio l_L/l_R is the super Janus solution. As demonstrated, for $0 < c_s < e^{A^*}$, the intervals on either side of the interface are given by equation (2.15). Solving for c_s , we obtain the following relation

$$c_s = \frac{\tanh\left[\frac{1}{2} \log(l_R/l_L) \operatorname{sech}(\theta) \operatorname{sech}(\psi)\right]}{\cosh \theta \cosh \psi}, \tag{2.47}$$

for general values of θ and ψ .

3 Constraints on $g_{\text{eff}}(l_L/l_R)$

It is particularly compelling to explore whether fundamental properties of entanglement entropy can yield valuable insights into the behavior of interface entropy and the effective central charge. One question one can explore is whether there is a constraint on the evolution of the effective quantities under RG flow when we deform the ICFT by a relevant deformation. In this case the length of the interval serves as a stand in for RG scale. This strategy has first been employed in [35] to derive the standard c -theorem of 2d CFTs only from basic properties of the EE. In addition we can ask whether we can use the same strategy to potential constrain the functional form of g_{eff} as a function of l_L/l_R already within the ICFT.

In principle, interface entropy bounds should reduce to boundary entropy constraints as discussed in [8]. We follow here a similar path and propose a g_{eff} -theorem for the interface entropy. This is further examined and verified within the framework of holography.

The derivation stems from one of the most significant constraints satisfied by entanglement entropy, that of strong subadditivity (SSA) inequality [35, 36] given by

$$\Delta S = S_A + S_B - S_{A \cap B} - S_{A \cup B} \geq 0. \quad (3.1)$$

For a holographic derivation of SSA see [27, 36].

We can consider a setup as figure 5, where A is defined by $[-l_a - l_c, l_a + l_c + \epsilon]$ and $B = B_1 \cup B_2$ defined by B_1 given by $[-l_a - l_b - l_c, -l_a]$ and B_2 given by $[l_a, l_a + l_b + l_c + \epsilon]$. Then, using the SSA inequality (1.3) we obtain

$$\begin{aligned} & \frac{c}{3} \log(2(l_a + l_c) + \epsilon) + \log g_{\text{eff}}(2(l_a + l_c) + \epsilon) + \frac{c}{3} \log(l_b + l_c) + \frac{c}{3} \log(l_b + l_c + \epsilon) \\ & \geq \frac{c}{3} \log l_c + \frac{c}{3} \log(l_c + \epsilon) + \frac{c}{3} \log(2(l_a + l_b + l_c) + \epsilon) + \log g_{\text{eff}}(2(l_a + l_b + l_c) + \epsilon). \end{aligned} \quad (3.2)$$

In the limit of $l_b \rightarrow 0$ we find that

$$\left. \frac{d}{dl} \log g_{\text{eff}} \right|_{l \equiv 2(l_a + l_c) + \epsilon} \leq \frac{c}{3} \left[\frac{1}{2(l_c + \epsilon)} + \frac{1}{2l_c} - \frac{1}{2(l_a + l_c) + \epsilon} \right]. \quad (3.3)$$

Taking the limit $l_a \rightarrow 0$ we find

$$\left. \frac{d}{dl} \log g_{\text{eff}} \right|_{l \equiv 2(l_a + l_c) + \epsilon} \leq \frac{c}{3} \left[\frac{1}{2(l_c + \epsilon)} + \frac{1}{2l_c} - \frac{1}{2l_c + \epsilon} \right]. \quad (3.4)$$

Employing the fact that $2l_c + \epsilon \equiv l$ we get

$$\left. \frac{d}{dl} \log g_{\text{eff}} \right|_{l \equiv 2(l_a + l_c) + \epsilon} \leq \frac{c}{6l} \frac{1 + (l_L/l_R)^2}{l_L/l_R}, \quad (3.5)$$

where we have defined $l_L = l_a + l_c$ and $l_R = l_L + \epsilon$ in this setup. Notice that (3.5) reduces to $\frac{c}{3l}$ for the boundary entropy, aligning with the results presented in [8]. Consequently, the derivative of the interface entropy $\log g_{\text{eff}}$ is bounded above by a positive quantity. Although this result does not suffice to establish the g_{eff} -theorem, it is fully compatible with the SSA constraint.

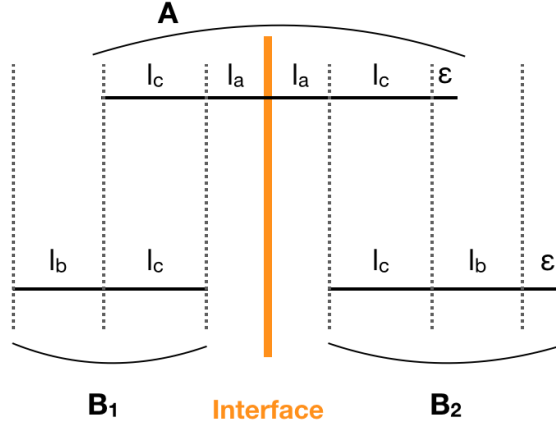


Figure 5. Time slice setup for the SSA analysis of g_{eff} -theorem.

3.1 Entropic g_{eff} -theorem

In order to have a well-defined g_{eff} -theorem we need to consider relativistic setups. Building on the approach outlined in [28], we explore the possibility of formulating a g_{eff} -theorem for ICFTs involving asymmetric intervals around the interface. Consider a 2D CFT with central charge c on the (x, t) -plane, where an interface is located at $x = 0$, as illustrated in figure 6. In addition, consider two causal regions $(-s, s)$ and (σ, σ) on the left and right of the timelike interface. The null rays emanating from these regions define a causal triangle, within which the intervals A_1, B_1 and A_2, B_2 lie. For the SSA analysis, we take $A = A_1 \cup A_2$ and $B = B_1 \cup B_2$. S_{int} denotes the entanglement entropy when one endpoint of the interval lies on the interface. The parameters $s, u, v, w, \sigma, \chi, \kappa$ and ϕ are appropriately chosen to extract the most stringent constraints from the SSA inequality.

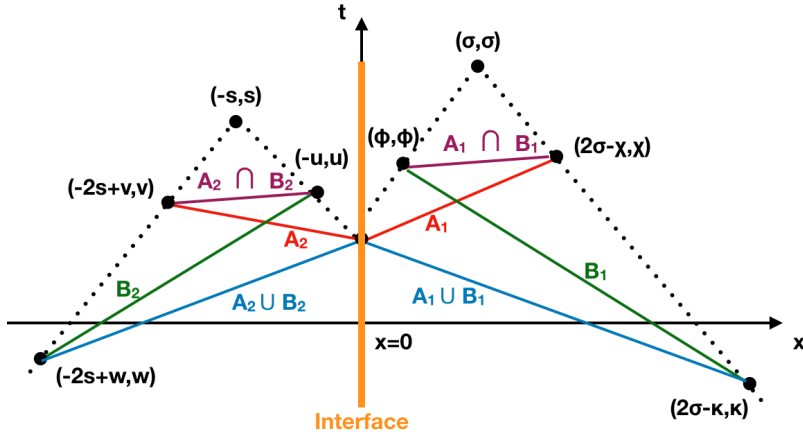


Figure 6. Lorentzian setup for the SSA in an ICFT₂ with asymmetric intervals around the interface.

We begin by considering the limits $u \rightarrow s$ and $\phi \rightarrow \sigma$. In this regime, the entanglement entropies associated with the individual intervals, their union, and their intersection are

expressed as follows

$$S_A = S_{\text{int}}(2\sigma - \chi) + S_{\text{int}}(2s - v), \quad (3.6)$$

$$S_{A \cup B} = S_{\text{int}}(2\sigma - \kappa) + S_{\text{int}}(2s - w), \quad (3.7)$$

$$S_B = \frac{c}{3} \log \left[\frac{16}{\epsilon^4} (\sigma - \phi)(\sigma - \kappa)(s - u)(s - w) \right], \quad (3.8)$$

$$S_{A \cap B} = \frac{c}{3} \log \left[\frac{16}{\epsilon^4} (\sigma - \phi)(\sigma - \chi)(s - u)(s - v) \right], \quad (3.9)$$

where $S_{\text{int}}(l) \equiv \frac{c}{3} \log \frac{l}{\epsilon} + \log g_{\text{eff}}$.

Next, we take the value v and χ very close to ω and κ respectively by using $v = \omega + \delta$ and $\chi = \kappa + \eta$, where δ and η are infinitesimally small and positive constants. Under these approximations, the SSA inequality takes the form

$$-\eta \frac{dS_{\text{int}}}{d\psi} \Big|_{\psi=2\sigma-\kappa} - \delta \frac{dS_{\text{int}}}{d\xi} \Big|_{\xi=2\sigma-\omega} + \frac{c}{3} \left(\frac{\eta}{\sigma - \kappa} + \frac{\delta}{s - w} \right) \geq 0. \quad (3.10)$$

Finally, we assume that $\omega, \kappa < 0$ and take both s and σ very small such that $s \ll |w|$ and $\sigma \ll |\kappa|$. Then, SSA provides the tightest bound given by

$$\eta \frac{d \log g_{\text{eff}}}{d\psi} + \delta \frac{d \log g_{\text{eff}}}{d\xi} \leq 0. \quad (3.11)$$

We consider two distinct cases for the interface entropy. The first case is to see whether we can find already non-trivial bounds within the ICFT before we deform with relevant operators to trigger RG running. In this case g_{eff} depends solely on the ratio $\rho \equiv \xi/\psi = l_L/l_R$. Under this assumption, equation (3.11) yields

$$\frac{d \log g_{\text{eff}}(\rho)}{d\rho} \leq 0, \quad (3.12)$$

given the condition $\rho < \frac{\delta}{\eta}$, which can always be satisfied. This monotonicity condition on g_{eff} as a function of the ratio l_L/l_R is consistent with the interface entropy for the super-Janus, RS braneworld and Janus solutions discussed in section 2.2, section 2.5 and [15] respectively, as advertised earlier. It also aligns with the analytic results for $\log g_{\text{eff}}$ in the super Janus case, where the relationship between c_s and the ratio is explicitly given by equation (2.47).

The second assumption we consider is that g_{eff} depends on both the ratio ρ and the total length $l \equiv \psi + \xi$ as would be appropriate if we trigger an RG flow by deforming the ICFT by a relevant deformation. In this case, we can rewrite the SSA condition as follows

$$\frac{\partial \log g_{\text{eff}}(\rho, l)}{\partial l} \leq \frac{(\rho - 1)}{2\psi} \frac{\partial \log g_{\text{eff}}(\rho, l)}{\partial \rho}. \quad (3.13)$$

Notice that for $\rho = 1$ (symmetric interval case), (3.13) reduces to

$$\frac{d \log g(l)}{dl} \leq 0, \quad (3.14)$$

which is the boundary entropy g -theorem, discussed in [28].

3.2 Holographic SSA

In this section we establish the g_{eff} -theorem within the holographic framework. To demonstrate this, we utilize the general expression for the interface entropy (2.44) in conjunction with the relation between the integration constant c_s and the interval ratio l_L/l_R (2.46). The former yields

$$\frac{d \log g_{\text{eff}}}{dc_s} = \frac{1}{4G_N} \int_{-r_c^-}^{r_c^+} \frac{c_s e^A}{(e^{2A} - c_s^2)^{3/2}} dr \geq 0. \quad (3.15)$$

Taking a derivative of (2.46) we obtain

$$\frac{d(l_L/l_R)}{dc_s} = -\frac{e^A e^{-\frac{c_s e^{-A}}{\sqrt{e^{2A} - c_s^2}}}}{(e^{2A} - c_s^2)^{3/2}} < 0, \quad (3.16)$$

demonstrating a monotonically decreasing behavior. It is easy to see that

$$\frac{d \log g_{\text{eff}}}{d(l_L/l_R)} \leq 0, \quad (3.17)$$

which proves the g_{eff} -theorem (3.12) in a holographic setup.

Acknowledgments

We thank Hare Krishna for useful discussions. The work of EA is supported by the Severo Ochoa fellowship PA-23-BP22-170 and partially supported by the AEI and the MCIU through the Spanish grant PID2021-123021NB-I00. The work of AK is supported in part by the U.S. Department of Energy under Grant No. DE-SC0022021 and a grant from the Simons Foundation (Grant 651678, AK). EA would like to thank the Weinberg Institute for the kind hospitality.

A Entropic quantities under KK compactification

In this appendix, we verify the statement that the 6D computations for the effective central charge c_{eff} [37] and the g -number [31] of super-Janus agree with the 3D computations in the KK reduced theory, first introduced in [21], which we used.

A.1 Boundary entropy g

The 6D g -number has been computed in [31] and is given by

$$S_{\text{bdy}}^{6D} = \frac{16\pi^2 L^2}{4G_6} \cosh^2 \psi \cosh^2 \theta \log(\cosh \psi \cosh \theta), \quad (A.1)$$

where G_6 is the six-dimensional Newton constant. We aim to rederive this result from a three-dimensional perspective. The KK compactification of the ten-dimensional super-Janus down to three dimensions was carried out in [21], where the three-dimensional metric is given by

$$ds_{(3)}^2 = R^2 \left(\frac{\cosh^2(r + \psi)}{\cosh^2 \theta \cosh^2 \psi} ds_{\text{AdS}_2}^2 + dr^2 \right) \quad (A.2)$$

with $R^2 = 2L \cosh \psi \cosh \theta$ is the AdS_3 radius. One needs to be careful with the regulated limits on the boundary. We obtain

$$\lim_{r \rightarrow \pm\infty} \frac{\cosh^2(r + \psi)}{\cosh^2 \theta \cosh^2 \psi} = \frac{e^{\pm 2(r + \psi)}}{4 \cosh^2 \psi \cosh^2 \theta} \implies \lambda_{\pm} = \frac{e^{\pm 2\psi}}{4 \cosh^2 \psi \cosh^2 \theta} \quad (\text{A.3})$$

We take $z = z_0$ and the length of the geodesic is given by

$$\Gamma(\theta, \psi) = \int ds = R \int dx = R(r_{\infty} - r_{-\infty}) \quad (\text{A.4})$$

with the regulated integration limits given by

$$r_{\infty} = -\log \epsilon - \frac{1}{2} \log \lambda_+ + \log 2z_0 \quad (\text{A.5})$$

$$r_{-\infty} = \log \epsilon + \frac{1}{2} \log \lambda_- - \log 2z_0 \quad (\text{A.6})$$

Then

$$\frac{\Gamma(\theta, \psi)}{R} = -2 \log \epsilon + 2 \log(\cosh \psi \cosh \theta) + 2 \log 2z_0 \quad (\text{A.7})$$

In order to compute the boundary entropy g , one needs to subtract the pure AdS contribution from the boundary entropy containing the interface. Therefore we have

$$\begin{aligned} S_{bdy}^{3D} &= \frac{\Gamma(\theta, \psi) - \Gamma(0, 0)}{4G_3} = \frac{2R}{4G_3} \log(\cosh \psi \cosh \theta) \\ &= \frac{2R^4 2\pi^2}{4G_6} \log(\cosh \psi \cosh \theta) \end{aligned} \quad (\text{A.8})$$

which is in agreement with (A.1). Here we have used the fact that the six-dimensional Newton constant is related to the three-dimensional one by $G_6 = G_3 V_3 = G_3 2\pi^2 R^3$, where V_3 is the volume of the compactified three-dimensional space.

A.2 Effective central charge c_{eff}

The six-dimensional effective central charge c_{eff} has been computed in [37] and is given by

$$S^{6D} = \frac{1}{\cosh \psi \cosh \theta} \frac{3 \times 32\pi^3 V_{M_4} L^2 \cosh^2 \theta \cosh^2 \psi}{\kappa_{10}^2} \frac{1}{6} \log \left(\frac{l}{\epsilon} \right) \quad (\text{A.9})$$

with Newton constant expressed as $\kappa_D^2 = 8\pi G_D^N$. Using the KK compactified three-dimensional metric as in [21], we obtain for the length of the geodesic

$$\Gamma(\theta, \psi) = \int ds = R \int dz \sqrt{\frac{\cosh^2(r + \psi)}{\cosh^2 \theta \cosh^2 \psi} \frac{1}{z^2} + (r')^2} \quad (\text{A.10})$$

The equations of motion admit a simple solution $r(z) = r_0$. The induced metric on this solution is given by

$$ds_{ind}^2 = R^2 \frac{\cosh^2(r_0 + \psi)}{\cosh^2 \theta \cosh^2 \psi} \frac{dz^2}{z^2} \quad (\text{A.11})$$

Therefore, the length of the geodesic

$$\Gamma(\theta, \psi) = \frac{R \cosh(r_0 + \psi)}{\cosh \theta \cosh \psi} \log \left(\frac{l}{\epsilon} \right) \quad (\text{A.12})$$

which is minimized at $r_0 = -\psi$. Therefore, the holographic entropy can be computed

$$\begin{aligned} S^{3D} &= \frac{\Gamma(\theta, \psi)}{4G_3} = \frac{R}{4 \cosh \theta \cosh \psi G_3} \log \left(\frac{l}{\epsilon} \right) \\ &= \frac{R^4 2\pi^2 V_{M_4}}{4 \cosh \theta \cosh \psi G_{10}} \log \left(\frac{l}{\epsilon} \right) \\ &= \frac{1}{\cosh \theta \cosh \psi} \frac{L^2 \cosh^2 \psi \cosh^2 \theta 2\pi^2 V_{M_4} 8\pi}{\kappa_{10}^2} \log \left(\frac{l}{\epsilon} \right) \\ &= \frac{1}{\cosh \theta \cosh \psi} \frac{3 \times 32\pi^3 V_{M_4} \cosh^2 \theta \cosh^2 \psi}{\kappa_{10}^2} \frac{1}{6} \log \left(\frac{l}{\epsilon} \right) \end{aligned} \quad (\text{A.13})$$

which agrees with the six-dimensional expression (A.9). Here we have employed the relation of the ten-dimensional Newton constant to the three-dimensional one, given by $G_{10} = G_3 V_{M_4} 2\pi^2 R^3$, with V_{M_4} being the volume of the four-dimensional internal manifold.

References

- [1] J.L. Cardy, *Effect of Boundary Conditions on the Operator Content of Two-Dimensional Conformally Invariant Theories*, *Nucl. Phys. B* **275** (1986) 200.
- [2] C. Bachas, J.d. Boer, R. Dijkgraaf and H. Ooguri, *Permeable conformal walls and holography*, *Journal of High Energy Physics* **2002** (2002) 027–027.
- [3] T. Quella, I. Runkel and G.M.T. Watts, *Reflection and transmission for conformal defects*, *JHEP* **04** (2007) 095 [[hep-th/0611296](#)].
- [4] M. Meineri, J. Penedones and A. Rousset, *Colliders and conformal interfaces*, *JHEP* **02** (2020) 138 [[1904.10974](#)].
- [5] P. Calabrese and J. Cardy, *Entanglement entropy and conformal field theory*, *Journal of Physics A: Mathematical and Theoretical* **42** (2009) 504005.
- [6] I. Affleck and A.W.W. Ludwig, *Universal noninteger ‘ground state degeneracy’ in critical quantum systems*, *Phys. Rev. Lett.* **67** (1991) 161.
- [7] S. Ryu and T. Takayanagi, *Aspects of holographic entanglement entropy*, *Journal of High Energy Physics* **2006** (2006) 045–045.
- [8] T. Azeyanagi, T. Takayanagi, A. Karch and E.G. Thompson, *Holographic calculation of boundary entropy*, *Journal of High Energy Physics* **2008** (2008) 054–054.
- [9] A. Karch and L. Randall, *Open and closed string interpretation of susy cft’s on branes with boundaries*, *Journal of High Energy Physics* **2001** (2001) 063–063.
- [10] K. Sakai and Y. Satoh, *Entanglement through conformal interfaces*, *JHEP* **12** (2008) 001 [[0809.4548](#)].
- [11] E.M. Brehm and I. Brunner, *Entanglement entropy through conformal interfaces in the 2D Ising model*, *JHEP* **09** (2015) 080 [[1505.02647](#)].

- [12] A. Karch and M. Wang, *Universal behavior of entanglement entropies in interface CFTs from general holographic spacetimes*, *JHEP* **06** (2023) 145 [[2211.09148](#)].
- [13] A. Karch, Y. Kusuki, H. Ooguri, H.-Y. Sun and M. Wang, *Universality of effective central charge in interface cfts*, 2023.
- [14] A. Karch, Y. Kusuki, H. Ooguri, H.-Y. Sun and M. Wang, *Universal Bound on Effective Central Charge and Its Saturation*, *Phys. Rev. Lett.* **133** (2024) 091604 [[2404.01515](#)].
- [15] A. Karch, Z.-X. Luo and H.-Y. Sun, *Universal relations for holographic interfaces*, *Journal of High Energy Physics* **2021** (2021) .
- [16] S. Chapman, D. Ge and G. Policastro, *Holographic complexity for defects distinguishes action from volume*, *Journal of High Energy Physics* **2019** (2019) .
- [17] T. Anous, M. Meineri, P. Pelliconi and J. Sonner, *Sailing past the end of the world and discovering the island*, *SciPost Physics* **13** (2022) .
- [18] D. Bak, M. Gutperle and S. Hirano, *Three dimensional Janus and time-dependent black holes*, *JHEP* **02** (2007) 068 [[hep-th/0701108](#)].
- [19] D. Bak, M. Gutperle and S. Hirano, *A dilatonic deformation of ads_5 and its field theory dual*, *Journal of High Energy Physics* **2003** (2003) 072–072.
- [20] A. Karch and L. Randall, *Locally localized gravity*, *Journal of High Energy Physics* **2001** (2001) 008–008.
- [21] S. Baig, A. Karch and M. Wang, *Transmission coefficient of super-janus solution*, 2024.
- [22] S. Ryu and T. Takayanagi, *Holographic derivation of entanglement entropy from the anti-de sitter space/conformal field theory correspondence*, *Physical Review Letters* **96** (2006) .
- [23] M. Rangamani and T. Takayanagi, *Holographic Entanglement Entropy*, Springer International Publishing (2017), [10.1007/978-3-319-52573-0](#).
- [24] J. Maldacena *International Journal of Theoretical Physics* **38** (1999) 1113–1133.
- [25] E. Witten, *Anti de sitter space and holography*, 1998.
- [26] E.H. Lieb and M.B. Ruskai, *A fundamental property of quantum-mechanical entropy*, *Phys. Rev. Lett.* **30** (1973) 434.
- [27] M. Headrick and T. Takayanagi, *Holographic proof of the strong subadditivity of entanglement entropy*, *Physical Review D* **76** (2007) .
- [28] J. Harper, H. Kanda, T. Takayanagi and K. Tasuki, *The g-theorem from strong subadditivity*, 2024.
- [29] E. D’Hoker, J. Estes and M. Gutperle, *Exact half-bps type iib interface solutions i: local solution and supersymmetric janus*, *Journal of High Energy Physics* **2007** (2007) 021–021.
- [30] M. Chiodaroli, M. Gutperle and D. Krym, *Half-bps solutions locally asymptotic to $ads_3 \times S^3$ and interface conformal field theories*, *Journal of High Energy Physics* **2010** (2010) .
- [31] M. Chiodaroli, M. Gutperle and L.-Y. Hung, *Boundary entropy of supersymmetric janus solutions*, *Journal of High Energy Physics* **2010** (2010) .
- [32] D. Bak, M. Gutperle and S. Hirano, *Three dimensional janus and time-dependent black holes*, *Journal of High Energy Physics* **2007** (2007) 068–068.

- [33] T. Takayanagi, *Holographic dual of a boundary conformal field theory*, *Physical Review Letters* **107** (2011) .
- [34] M. Gutperle and J. Samani, *Holographic renormalization group flows and boundary conformal field theories*, *Physical Review D* **86** (2012) .
- [35] H. Casini and M. Huerta, *A finite entanglement entropy and the c-theorem*, *Physics Letters B* **600** (2004) 142–150.
- [36] T. Hirata and T. Takayanagi, *Ads/cft and strong subadditivity of entanglement entropy*, *Journal of High Energy Physics* **2007** (2007) 042–042.
- [37] M. Gutperle and J.D. Miller, *Entanglement entropy at holographic interfaces*, *Physical Review D* **93** (2016) .